

A comparison of detailed equatorial red bed records of secular variation during the Permo-Carboniferous Reversed Superchron

Marcela M. Haldan,¹ Cor G. Langereis,¹ Andrew J. Biggin,¹ Mark J. Dekkers¹ and Michael E. Evans²

¹*Paleomagnetic Laboratory Fort Hoofddijk, Utrecht University, Budapestlaan 17, 3584 CD, Utrecht, the Netherlands. E-mail: haldan@geo.uu.nl*

²*Institute for Geophysical Research, University of Alberta, Edmonton, T6G2J7, Canada*

Accepted 2009 January 15. Received 2008 December 1; in original form 2008 April 1

SUMMARY

Detailed secular variation records during a superchron may provide information on the behaviour of the geodynamo during periods that the field does not reverse. The Permian red beds in Dôme de Barrot (southern France)—deposited during the Permo-Carboniferous Reversed Superchron (PCRS, 317–265 Ma)—were previously argued to accurately record palaeosecular variation (PSV). This result is particularly valuable because the red beds were deposited near the palaeo-equator and therefore, according to one model of secular variation, determine the contribution of the even (symmetric) spherical harmonics of the field.

We have extended the Dôme de Barrot sequence, and we have established a new record from the Permian red beds from the Lodève basin (southern France), also deposited at low latitudes. Additionally, we critically review published data from low latitude Permian red beds from the same basins. We focus on records with a sufficient number of samples, and acquire, whenever possible, the original data, or—as a second choice—parametrically sampled published site means. We test the distributions of these directions using a statistical secular variation field model (TK03.GAD). The angular standard deviation (ASD) of the virtual geomagnetic pole (VGP) distribution is a measure of (palaeo)secular variation, and we compare our values of ASD from the Permian red beds to those from lavas erupted in the last 5 Myr. Contrary to our previous studies, we now conclude that secular variation during the Permo-Carboniferous Reversed Superchron is slightly, but significantly, reduced at low latitudes compared with the recent field, as based on a latest compilation that supercedes earlier compilations. It also agrees with a new study, which found that PSV, at low palaeolatitudes during the Cretaceous Normal Superchron, was also significantly lower than in periods with frequent reversals.

Key words: Palaeomagnetic secular variation; Rock and mineral magnetism; Europe.

1 INTRODUCTION

Detailed and reliable records of the geomagnetic field through geological time are crucial to our understanding of the geodynamo and its long-term behaviour. This involves, for example, changes in reversal frequencies and the behaviour of the field at plate tectonic and mantle convection timescales, typically of the order of tens of millions of years, but it also includes detailed short-term records of the field at distinct geological time intervals.

In the absence of long and continuous geomagnetic records for increasingly older periods of the geological timescale, high resolution and high quality records of short time intervals during Earth's history may provide useful information on the long-term behaviour of the field and may, thus, provide clues that improve our understanding of the geodynamo. The geodynamo is generated by convection in the fluid outer core, although the behaviour of the geomagnetic field also strongly depends on the solid inner core (Hollerbach &

Jones 1993; Coe & Glatzmaier 2006). Knowledge of palaeosecular variation (PSV) behaviour is important because it constrains geodynamo models. For example, models with different thermal conditions at the core–mantle boundary (Glatzmaier *et al.* 1999; Coe & Glatzmaier 2006) show distinctly different pattern of PSV with latitude (Tauxe *et al.* 2008). The character of PSV can be defined in several ways: by visualization using Bauer (declination versus inclination) plots; by analysing the distribution of characteristic remanent magnetization directions (ChRM) or their corresponding virtual geomagnetic poles (VGPs) and their latitudinal dependence or by analysis of the power spectrum of different intervals of the field (Kruiver *et al.* 2002; Constable & Johnson 2005). A method well accessible to palaeomagnetism is determining the latitude dependence of the angular standard deviation (ASD) of either the palaeomagnetic directions or of their corresponding VGPs (McFadden *et al.* 1988; McElhinny & McFadden 1997), the latter ASD commonly referred to as ‘VGP scatter’. In palaeomagnetism,

it is common to transform field directions into VGPs by using the equations for a geocentric axial dipole (GAD). The variations in angular dispersion as a function of latitude calculated in these two ways are quite different and have been discussed in detail by Cox (1970). See McElhinny & Merrill (1975) for a review of early (lava) records and statistical PSV field models. For the Cretaceous Normal Superchron (CNS), for example, McFadden *et al.* (1991) determined the ASD from lavas, and they argued that VGP scatter at low palaeolatitudes was lower during that time interval. The dynamo could then be in a ‘steady’ (stable) state, in contrast to the ‘oscillatory’ (unstable) state, a period with frequent reversals like during the past tens of millions of years (McFadden & Merrill 1995). During the past two decades, the nature of the geomagnetic field has been extensively studied through more advanced statistical PSV models based on a Giant Gaussian Process (GGP; Constable & Parker 1988; Quidelleur & Courtillot 1996; Tauxe & Kent 2004). The most recent compilation of lava records for the past 5 Myr and a comparison with GGP models was carried out by Johnson *et al.* (2008). Finally, several studies have ‘sampled’ geodynamo models based on numerical simulations (Glatzmaier & Roberts 1995; Glatzmaier *et al.* 1999; Glatzmaier & Olson 2005; Coe & Glatzmaier 2006) and compared the results with observed field behaviour (Coe *et al.* 2000; Brown *et al.* 2007; Valet & Plenier 2008).

Palaeomagnetism is the only method that permits the long-term history of the geomagnetic field to be obtained. Superchrons are long periods of time (tens of million of years) characterized by an absence of geomagnetic reversals. Their occurrence on plate tectonic timescales suggests the influence of mantle convection processes. In Earth’s history, two superchrons are well known, namely, the CNS from 124 to 84 Ma (Ogg *et al.* 2004) and the Permo-Carboniferous Reversed Superchron (PCRS) from 317 to 265 Ma (Opdyke *et al.* 2000; Menning *et al.* 2001; Menning *et al.* 2006). Alternatively, frequency of reversals can be discussed in terms of the contribution of the odd/even harmonics of the field through time (McFadden *et al.* 1991; Coe & Glatzmaier 2006). A critical factor in all these models is the timescale of the different processes that play a role in the geodynamo, for example, the magnetic diffusion time of the inner core, mantle overturn times, heat flux distribution at the core–mantle boundary and also on the rate of inner core growth (Biggin *et al.* 2008a).

Records of the geomagnetic field can be obtained from igneous rocks and from sedimentary sequences. Sedimentary sequences have the advantage of offering continuous high resolution records of the natural remanent magnetization (NRM), but they are often flawed by the processes governing NRM acquisition. Nevertheless, it has been shown earlier (Maillol 1992; Maillol & Evans 1993; Kruiver *et al.* 2000) that red beds can be excellent recorders of the geomagnetic field, especially, if the they are of detrital rather than of diagenetic, chemical origin.

Very few good (with a large number of samples) and detailed sedimentary records of the geomagnetic field during the PCRS are available, and those with a sufficient number of samples ($N > 100$), which adequately sample the field, are very rare. In addition, the records may be biased because of sedimentary artefacts. An important artefact is the inclination error, which can lead to a shallowing of the acquired NRM because of compaction or other depositional processes (Tauxe & Kent 1984). Several other factors may influence the recording of the field, like (partial) remagnetization, late diagenesis or the contamination by a younger overprint. A possible contribution of an octupole field to the total field causing seemingly lower inclinations (Kent & Smethurst 1998; Van der Voo & Torsvik 2001) will disturb the nature of the observed ChRM or VGP distri-

bution, which is usually taken to represent a GAD field. Also, an age assignment that is too young or too old because of poor age control or new developments in the geological timescale (Van der Voo & Torsvik 2001; Gradstein *et al.* 2004) may hamper temporal comparison of spatially different records.

The purpose of this paper is to present large PSV data sets of red beds deposited during the PCRS at low latitudes. We provide a new detailed record (Lodève basin, France—one of the most complete and best exposed Permian red bed basins in Europe) as well as an extended record (Dôme de Barrot, France) to assess the comparability of these PSV records, which are approximately time equivalent. We compare our new record from the Lodève basin with the study of Kruseman (1962) [who used alternating field (AF) demagnetization], Maillol (1992) and with other existing records (Merabet & Guillaume 1988; Cogné *et al.* 1990) with a too small number of samples, and we augment the data sets with a large number of new measurements. An additional purpose of this study is to compare our Lodève record with the extended Dôme de Barrot record (Van den Ende 1970; Kruiver *et al.* 2000) and to assess if these red beds from different basins and with different magnetic properties give reliable and comparable results in terms of sampling PSV. We performed extensive rock magnetic methods to test the reliability of the NRM acquisition in these red beds. We will argue that the red bed records from Lodève and Dôme de Barrot provide useful constraints on PSV behaviour. Since they provide high-resolution palaeomagnetic records during the PCRS, they will enable us to compare these records with other sedimentary records from the literature. An assessment and compilation of all globally distributed sedimentary records from the PCRS, however, will be the subject of a subsequent paper.

A third reason for this study was to investigate PSV behaviour, specifically at low latitudes, since it has been suggested that especially the contribution of the even (or symmetric) spherical harmonics to the field (‘quadrupole family’ in older literature) would be significantly lower during a superchron (McFadden & McElhinny 1988; McFadden *et al.* 1991). Here, we investigate PSV by analysis of the VGP scatter, and we compare the results with the PSV for the last 5 Myr (McElhinny & McFadden 1997; Johnson *et al.* 2008). For large enough data sets ($N > 100$), we first applied the statistical field model TKO3.GAD (Tauxe & Kent 2004), both for correction of the inclination error and for assessing the shape of the directional distributions. Our results indicate, overall, that PSV during the PCRS is lower than today at low latitudes, in agreement with the recent results from the CNS (Biggin *et al.* 2008b).

2 GEOLOGICAL SETTING

The red beds from Lodève and Dôme de Barrot were deposited during the PCRS near the palaeo-equator.

2.1 Dôme de Barrot

The Dôme de Barrot is situated in southeastern France (6°48′E and 44°07′N, Fig. 1a) in the external zone of the French Alps. Two formations can be distinguished (Bordet 1950): the Daluis Formation and the Leouvé Formation. The rocks in the northwestern part of Dôme de Barrot are undeformed, but deformation increases to the east. The provenance area of the red bed material is situated west, south or east of the Dôme de Barrot and provided large quantities of volcanoclastic products. The bedding plane at the sampling site (Fig. 1a), dips gently (12°) to the north.

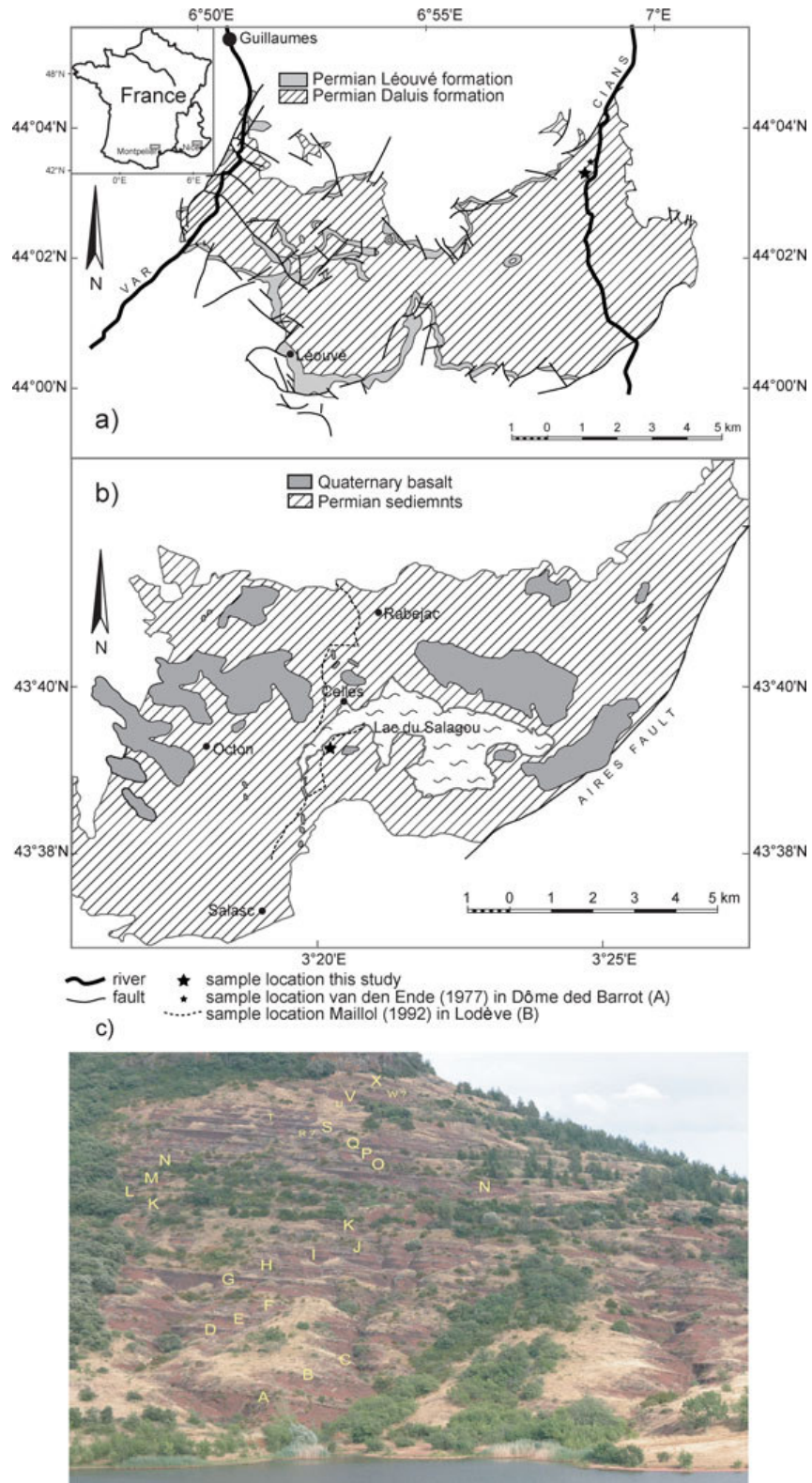


Figure 1. Simplified geological map of Dôme de Barrot (a), Lodève basin (b) and the typical ‘cyclical’ outcrop of the Octon Member, north of Lake Salagou (c); the prominent silty layers are denoted by letters.

Table 1. Summary of published ages and new ages according to Schneider *et al.* (2006) for this and other, published studies.

Nr.	Study	Published age	New age	New age (Ma)
Dôme de Barrot				
1	Dôme de Barrot, this study		Roadian	272.5–268
2	Kruiver <i>et al.</i> (2000)	Roadian	Roadian	272.5–268
3	Van den Ende (1977)	Early Thuringian	Roadian	272.5–268
Lodève				
4	Lodève, Salagou Fm. (Octon Mb.), this study		Kungurian	279.5–272.5
4*	Maillol (1992), Salagou Fm. (Octon Mb. and Merifons Mb.)	Thuringian	Kungurian–Wordian	279.5–265
5	Maillol (1992), Viala Fm. and Rabejac Fm.	Thuringian	Sakmarian–Artinskian	287.5–279.5
6	Kruseman (1962), Rabejac Fm. and Salagou Fm. (Octon Mb.)	Saxonian	Artinskian–Wordian	284–265
7	Kruseman (1962), Viala Fm.	Autunian	Sakmarian	290–284
8	Mérabet & Guillaume (1988), Rabejac Fm. and Salagou Fm. (Octon Mb.)	Saxonian	Artinskian–Wordian	284–265
9	Mérabet & Guillaume (1988), Viala Fm.	Autunian	Sakmarian	290–284
10	Cogné <i>et al.</i> (1990), Rabejac Fm. and Salagou Fm.	Autunian	Kungurian–Wordian	279.5–265

Notes: The youngest possible numerical age in the table is 265 Myr, that is, the end of the PCRS (Opdyke *et al.* 2000), since all studies report reversed directions. Numbers refer to those used in Table 2 and Fig. 7, where 4 occurs twice (4 and 4*) because our study (4) has been combined with the younger part of data of Maillol (1992)

The age of Dôme de Barrot can be constrained by the palynological data from the Leouvé Formation, which forms the top of the Dôme de Barrot sequence. Visscher *et al.* (1974) assigned a Late Permian age to the pollen from intercalations of grey siltstones in the red beds (Van den Ende 1970). However, more recently, a Guadalupian (Roadian; see Table 1) age (Glenister *et al.* 1999) was assigned to the pollen (Kruiver *et al.* 2000). Since the end of the PCRS is dated at 265 Ma (Opdyke *et al.* 2000), the Dôme de Barrot red beds must have been deposited during a period in the youngest part of the PCRS. Earlier, it was found that the entire sequence is of reversed polarity (Kruiver *et al.* 2000). The earliest study of Dôme de Barrot was done by Van den Ende (1970, 1977), the latest by Kruiver *et al.* (2000), who show that the NRM of the red beds of Dôme de Barrot resides in detrital, specular haematite of volcanic origin.

We have extended the record (by ~1.5 m) of Kruiver *et al.* (2000) in the Daluis Formation, consisting of dark red mudstones (1.5–3.0 m) intercalated with purple siltstones (0.1–0.5 m) and, additionally, increased the resolution of this earlier record by drilling in between the previously taken cores. This reduced the average sample spacing of 2–3 cm to the ~1 cm scale. In total, we drilled 116 cylindrical samples with a diameter of 2.5 cm. The sedimentation rate is well known (~12 cm kyr⁻¹) because the susceptibility record unambiguously shows orbital frequencies (Kruiver *et al.* 2000). We use the same susceptibility record here but apply a slightly different spectral analysis (Paillard *et al.* 1996). We compare the ratios of spectral peaks in the record with those derived from the summer insolation series at 65°N (Laskar 1990) (Fig. 2). Since the orbital ratios change throughout geological time (Berger *et al.* 1992), with the period of eccentricity remaining virtually constant and the periods of obliquity and precession decreasing, we determine the linear regression coefficients between the peaks in our susceptibility record—very similar to Quaternary records (King 1996)—and the orbital peaks. Effectively, we compare the ratios of our record with the orbital ratios back in time—and find a best fit very close to the end of the PCRS, in remarkable agreement with our age assignment.

2.2 Lodève basin

The Lodève basin is situated on the southern border of the Massif Central (43°41.5'N, 3°21'E, Fig. 1b). The basin corresponds to a

zone of subsidence, its monoclinical filling dips to the south at an average angle of 12°. The general structure of the basin is that of a half-graben, controlled by major faults to the south (Aires fault) and to the east (Cevennes fault). Permian sediments crop out in an area of 150 km², with a total thickness of approximately 2500 m, and they have a volcanic detrital content (Schneider *et al.* 2006). The recent study of Schneider *et al.* (2006) on the Permian climate history in the Lodève basin has enabled the correlation of this record to other European and global Permian records, which has resulted in a significantly improved age model for the Lodève basin formations and members. Numerical ages are based on the Permian timescale of Menning *et al.* (2006). We have adopted this age model and applied it to other published records as well (Table 1).

The earliest study in Lodève was done by Kruseman (1962), who used only AF demagnetization to study the NRM. Many years later, Maillol (1992) studied the same Permian red beds. He argued that the NRM was a post-depositional remanent magnetization (pDRM). Haematite can carry either a depositional remanent magnetization (DRM) or a chemical remanent magnetization (CRM), or a mixture of both. In the case of a (p)DRM, the magnetization is acquired during (DRM) or shortly after (pDRM) deposition and can provide reliable records of the geomagnetic field (Steiner 1983; Tauxe & Badgley 1984). Although recorded directions residing in detrital haematite may show a large scatter in declinations as well as a pervasive inclination shallowing (Tauxe & Kent 1984), the original field declination—provided a sufficient number of samples is taken—is well preserved, and inclination shallowing can often be corrected successfully, also in continental deposits, using the elongation/inclination (*E/I*) method (Krijgsman & Tauxe 2004; Tauxe & Kent 2004; Kent & Tauxe 2005; Tauxe *et al.* 2008), discussed in more detail below.

We have extended the records of Maillol (1992), who sampled the lower and upper Salagou Formation (Octon Member and Mérifons Member) and the Rabejac Formation, and also the record of Kruseman (1962) by sampling the lower Salagou Formation (Octon Member). Cycles of the Octon Member consists of m-thick red brown siltstones and cm-thick calcareous siltstones. Sedimentary cycles of the Mérifons Member, consist of cm- to dm-thick red brown siltstones and grey-green cm thick siltstones with calcareous cements. These red beds seem to be sensitive to environmental change, and we might assume that the sedimentation pattern is influenced by climate, because field observations of the cyclicity

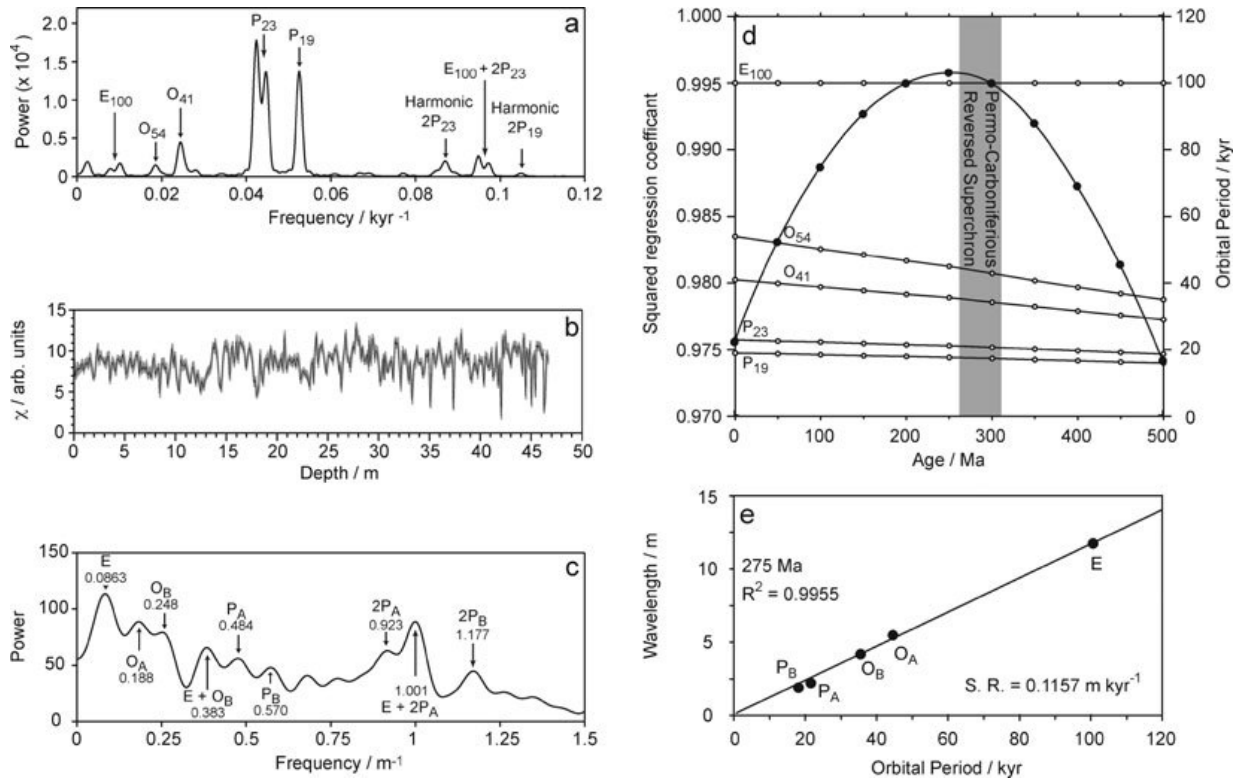


Figure 2. (a) Frequency spectrum (Paillard *et al.* 1996) obtained for truncated summer insolation $La_{90(1.1)}$ at 65°N (Laskar 1990). E , O and P labels represent eccentricity, obliquity and precession, respectively, and are suffixed with their periods (in kyr). Three peaks occur in the so-called ‘semi-precession’ band, two of which correspond to the 2nd precession harmonics (labelled $2P_{23}$ and $2P_{19}$), and the third is a combination peak resulting from the interaction of the eccentricity cycle with the 2nd harmonic of the 23 kyr precession ($E_{100} + 2P_{23}$). (b) Low-field magnetic susceptibility log (χ) record of Kruiwer *et al.* (2000). Each sample was a measure of total of 10 times and is represented by a mean value (black line) with $\pm 1\sigma$ errors (shaded region). (c). The ratios of the peak frequencies in the Dôme de Barrot χ spectrum allow the peaks to be assigned as eccentricity, obliquity, precession (including harmonics) and combination frequencies. Absolute periods cannot, however, be assigned to these peaks, so the E , O and P allocations are suffixed A , B etc. The $E + O_B$ combination peak observed at $f = 0.383 \text{ m}^{-1}$ is believed to correspond to the 29 kyr cycle $[(1/100) + (1/41) \approx 1/29]$, which has been reported in a number of Quaternary palaeoclimatic records (e.g. King 1996). (d) Quality of fit (closed symbols) by calculating the squared regression coefficients between the orbital periods varying through geological time (open symbols) and the wavelengths of the climatic oscillations isolated in the χ record (forced through the origin). E , O and P represent eccentricity, obliquity and precession, respectively, and are suffixed with their present-day periods in kyr. (e) Fit of χ wavelength and orbital periods for the spectral peaks defined in (b) after age assignment of 275 Myr for the studied sequence.

(Fig. 1c) suggest orbital forcing. Unfortunately, the observed sedimentary cyclicity cannot be unambiguously linked to orbital periods of precession, obliquity and eccentricity, since spectral analysis of a high-resolution susceptibility record (Figs 2 and 5) of the entire section (of Fig. 1c) fails to reveal the orbital ratios that are typical for the Permian. The most prominent cycle is, on average, 6 m thick; if this cycle represents precession, it would point to a sedimentation rate of approximately $\sim 30 \text{ cm kyr}^{-1}$. In any case, from the type of sediments in the Lodève basin—continental fluvial–lacustrine and alluvial fan red beds (Schneider 2006)—we argue that the sedimentation rate must be higher than that in the Dôme de Barrot—distal flood plain deposits—with a well-known sedimentation rate of $\sim 12 \text{ cm kyr}^{-1}$. Six large oriented sample blocks (hand samples) from different layers in the lower part of the section were sampled; the middle and upper part of the section contained sediments too fragile to be drilled in the field (see also Maillol 1992; Maillol & Evans 1993). In the laboratory, cylindrical samples with a diameter of 2.5 cm were drilled from these blocks, with an average spacing of 1–2 cm. This series consists of 88 samples with a very high time resolution.

3 METHODS

The characteristic remanent magnetizations (ChRM) of the Lodève and Dôme de Barrot series were determined by thermal demagnetization (TH), conducted with steps of 100°C up to 300 or 400°C ; for higher temperatures up to a maximum of 680°C , the intervals were reduced (to 50°C and down to 10°C) to permit a more detailed study of the NRM. The magnetization was measured on a horizontal 2G Enterprises DC-SQUID magnetometer (noise level $3 \times 10^{-12} \text{ A m}^2$). In addition to the directional characteristics, the unblocking temperatures of the different components were inferred from the thermal decay curves of the NRM.

In addition to palaeomagnetic analyses, the magnetic mineralogy was assessed with rock magnetic means. A MicroMag Model 2900 alternating gradient magnetometer was used, equipped with a 2 T magnet—but effectively 1.6 T because of partial saturation of the pole shoes—(Princeton Measurements Corporation, noise level $2 \times 10^{-9} \text{ A m}^2$). Successively, hysteresis loops, first-order reversal curves (FORC) and isothermal remnant magnetization (IRM) curves were measured, all at room temperature.

For each FORC diagram, 200 reversal curves were measured with an averaging time of 2 s per data point. For Lodève samples, two runs per sample were performed: (1) with low coercive force (B_c) values (0–150 mT) to detect magnetite and maghemite; (2) with high B_c values (0–1.6 T) to detect haematite. For Dôme de Barrot samples, one run (0–1.6 T) per sample was performed to detect haematite. FORC diagrams appeared to be fairly noisy, and since, especially, in the Dôme de Barrot samples saturation could not be reached in the available fields, we will not consider them any further.

Hysteresis loops and IRM acquisition curves of 14 representative samples were measured for the Lodève record and 13 samples for the Dôme de Barrot record. The IRM curves were decomposed into coercivity components using the IRM fitting method of Kruiver *et al.* (2001) that is limited to symmetric distributions in log-space. The interpretation of the diagrams for all samples provides a best-fit of one or two components, which have overlapping coercivity spectra. Each magnetic component can be characterized by the saturation IRM (SIRM), the peak field, at which half of the SIRM is reached ($B_{1/2}$) and the dispersion of its corresponding cumulative log-normal distribution (DP; Kruiver *et al.* 2001). Although the method of Egli (2004) allows for recognition of non-symmetrical (skewed) distributions, the coercivities of the major components in both methods are found to be essentially identical (Spassov *et al.* 2003). The small component with a low coercivity that is often observed in the Kruiver *et al.* method arises from this skewed data distribution—it has no physical meaning (Heslop *et al.* 2004).

Thermomagnetic runs were measured (nine representative samples for Lodève and five for Dôme de Barrot) in air with a modified horizontal translation type Curie balance (Mullender *et al.* 1993), with a sensitivity of $\sim 5 \times 10^{-9}$ A m². Approximately 30 mg of powdered samples were put into a quartz glass sample holder and were held in place by quartz wool; heating and cooling rates were 10 °C min⁻¹; measurements were made up to 700 °C. At selected temperatures during the heating, the temperature was lowered by 100 °C before heating to more elevated temperatures to check for chemical alterations during the analysis. Curie temperatures were determined with the two-tangent method (Grommé *et al.* 1969).

In Dôme de Barrot, magnetic susceptibility (χ) was measured on a profile of 48 m with a Bartington 2F sensor (sensitivity $\sim 10^{-6}$ SI) by Kruiver *et al.* (2000). It provides evidence for Milankovitch cycles (and their ratios) during the Permian, which we use here, to confirm the earlier estimate of sedimentation rate of 11.6 cm kyr⁻¹, and to derive an age estimate (Fig. 2). In Lodève, magnetic susceptibility (χ) was measured on the outcrop using a ZH Instruments SM 30 sensor (50 mm diameter, sensitivity $\sim 10^{-7}$ SI) by placing the probe on the flat, fresh-rock surface. The penetration depth of this sensor is 1–2 cm below the rock surface. A 150 m long profile was recorded in the Lodève basin at Salagou Lake (the section of Fig. 1c), with an average measurement spacing of 15 cm. The readings of the SM 30 field probe were used as a relative measure of χ .

For large enough data sets ($N > 100$), we applied an inclination error correction, using the *E/I* method based on the field model TK03.GAD (Tauxe & Kent 2004). This model is based on the assumption that the time-averaged field closely approximates that of a GAD. From the—essentially circular—VGP distribution generated by the model, it predicts the shape of the distribution of directions at any latitude (or equivalently, in the GAD assumption, for any corresponding inclination I) expressed by an elongation factor E , defined

as the ratio of the eigenvalues τ_2 and τ_3 of the directional distribution. In nature, the predicted directional distribution—elongated with a N–S directed E close to 2.9 at the equator and close to 1.0 at latitudes close to the pole—is often deformed (flattened), caused by DRM processes (King & Rees 1966; Tauxe & Kent 1984) or compaction effects (Blow & Hamilton 1978). The resulting sedimentary inclination error may cause the flattening of the distribution with a corresponding flattening factor f , thereby reducing the elongation E . King (1955) shows that f relates the observed inclination (I_o) and applied field inclination (I_f) as

$$\tan(I_o) = f \tan(I_f) \quad (1)$$

In practice, we ‘unflatten’ our observed directional distribution in small steps, by inverting (1), with values of f ranging from 1.0 (no flattening) to 0.3 (severe flattening). The average inclination I_f and elongation E_f of the increasingly unflattened distribution are calculated at each step, until the E_f / I_f ratio agrees with the model value. The corresponding inclination may then be taken as the original inclination, provided, of course, that we have a ‘reasonable’ distribution to start with, because many other factors than inclination shallowing alone, may have caused a distribution to be deformed beyond repair.

We found that the *E/I* correction has a negligible effect on the amount of VGP scatter itself, but it allows one to assess the directional distribution in terms of its predicted shape, whereas the corrected inclination allows one to provide a better estimate of the (simultaneously corrected) palaeolatitude versus the corresponding VGP scatter. Here, we use the TK03.GAD model with the new coefficients of Tauxe *et al.* (2008) in the *E/I* equation, rather than the old coefficients of Tauxe & Kent (2004); there is no noticeable difference (at most a few tenths of a degree).

PSV can be characterized by VGP scatter, that is, the angular dispersion S expressed as the ASD around the mean of the VGP distribution. All directions were transformed to VGPs, which are shown with respect to their mean (Fig. 7; Fig. S1) and the corresponding values of S were calculated; upper (S_u) and lower (S_l) error limits (95 per cent level) were calculated using a (5000 \times) bootstrap approach. VGP cut-offs are required to remove outlier data, which will otherwise dominate the measured ASD, and to enable comparison with published results. These outliers may be geomagnetic in origin (i.e. from excursions or reversal transitions), or they may be produced by errors associated with the sample properties or sampling and measurement process. There are three main ways of treating outliers: no cut-off, fixed cut-off and variable cut-off. The second excludes all VGPs that are more than a certain specified angular distance (usually 45°) from the mean pole, whereas the third, under certain assumptions about the underlying distribution, derives this cut-off angle from the data set itself.

We determine S by using a variable cut-off angle defined by Vandamme (1994); the optimal cut-off angle is calculated for each record by iteration. This has been argued to be a better estimate than using a fixed cut-off angle (McElhinny & McFadden 1997). The resulting VGP scatter can then be compared to, for instance, the scatter at certain latitudes during the last 5 Myr or during any other period. In principle, the Vandamme method permits a considerable improvement to the VGP scatter estimate characterising PSV, especially, for low and high latitudes—where a fixed cut-off angle tends to over- and underestimate the ASD, respectively—but it may perform rather unevenly, depending on the characteristics of the data set (Tauxe *et al.* 2008). In some cases, we determine whether two distributions have a common true mean direction. For this, we use

the method of McFadden & McElhinny (1990) in their reversal test. We have modified the software to accommodate also the test to distributions with the same polarity. We use Monte Carlo simulation, thereby effectively applying the Watson (1983) V_w statistic test. We determine γ , the angle between the means, and γ_c , the critical angle in the test. If $\gamma > \gamma_c$ the test is positive and the distributions share a common true mean direction. The quality of the test is expressed as A, B, C or indeterminate, depending on the value of γ_c (McFadden & McElhinny 1990).

4 RESULTS

4.1 Magnetic mineralogy

4.1.1 Thermomagnetic analysis

The results for the samples from Dôme de Barrot (sample MD 18; Fig. 3) are identical to our earlier study and show haematite with a Néel temperature close to 680 °C. The magnetization of the cooling curve is higher than the warming curve because at low temperatures, the haematite was not saturated by the cycling field of 150–300 mT (de Boer & Dekkers 1998). For the samples from the Lodève basin (sample B1.2; Fig. 3) Curie points of 640–650 °C are found, which is too high for magnetite. This may point to (thermally stable) maghemite or fine grained haematite. An inflection can be seen on the cooling curve but not on the warming curve, suggesting that a new magnetic phase with a Curie temperature of ~530 °C was formed during heating. Similar to the observations made by Boer & Dekkers (2001), this may be a maghemite type with some of the lattice vacancies on tetrahedral sites.

4.1.2 Hysteresis loops

Representative hysteresis loops are shown in Fig. 3. The curves were measured up to 2.0 T, and they are not saturated in these fields. We use standard slope correction (the highest 30 per cent of the maximum applied field, default setting of the MicroMag software), and we show only the part up to 1.6 T. The shape of the hysteresis loop for the samples from Dôme de Barrot (sample MD41; Fig. 3) has an open form, typical of single domain magnetic behaviour, but not yet saturated, which indicates the presence of a mineral with high coercivity. A B_{cr} value of ~700 mT (with respect to 1.6 T) is again indicating haematite presence in these samples.

The wasp-waisted shape of the hysteresis loop of the Lodève samples (Fig. 3) indicates the coexistence of two coercivity fractions (Roberts *et al.* 1995; Tauxe *et al.* 1996). The coercivity of remnance (B_{cr} with respect to 1.6 T obtained from backfield curve measurements) has a value of ~380 mT and is the weighted result of the contributions of the high- and low-coercivity fractions. Maghemite and magnetite are typified by values of a few tens of mT and ‘classical’ specular haematite by values of a few hundreds of mT (Dunlop & Özdemir 1997). A B_{cr} of ~380 mT is too high for maghemite/magnetite and is too low for haematite (although some pigmentary haematites have these values). Therefore, this value is likely the result of both carriers—maghemite/magnetite and haematite—as is suspected from the IRM component analysis (as discussed below).

4.1.3 IRM acquisition curves

The IRM acquisition curves contain 200 data points; examples of representative samples are given in Fig. 4, for which the fitted IRM

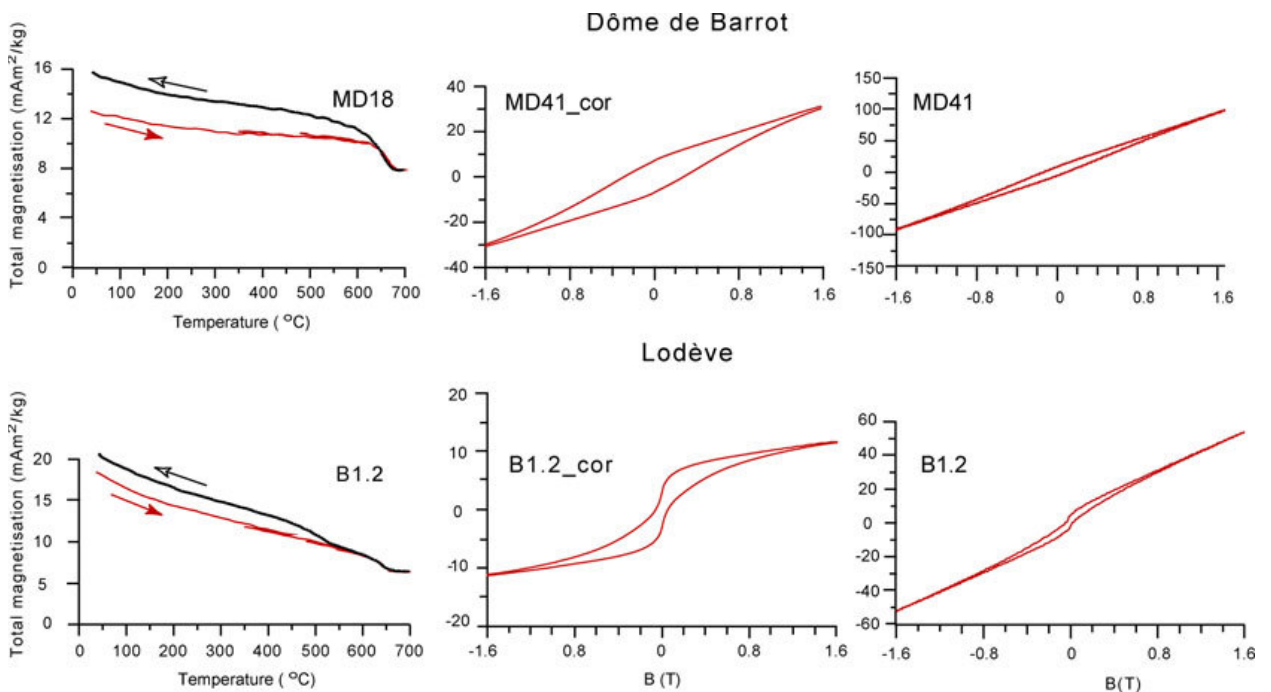


Figure 3. Representative thermomagnetic curves for powdered samples (approximately 30 mg) of different heating (red, solid lines) and cooling (black, dotted lines) runs, performed in air and at a rate of 10 °C min^{-1} (left-hand panels) and hysteresis loops—corrected for high-field slope (between 1.4 and 2.0 T) on a mass-specific basis—for characteristic samples from Dôme de Barrot and Lodève basin (right-hand panels). Because of saturation of the pole shoes at higher fields above 1.6 T, we show only the loops between -1.6 and $+1.6$ T. Since slope correction of unsaturated samples may give meaningless values for (remanent) saturation remanence and coercivities, we report no values.

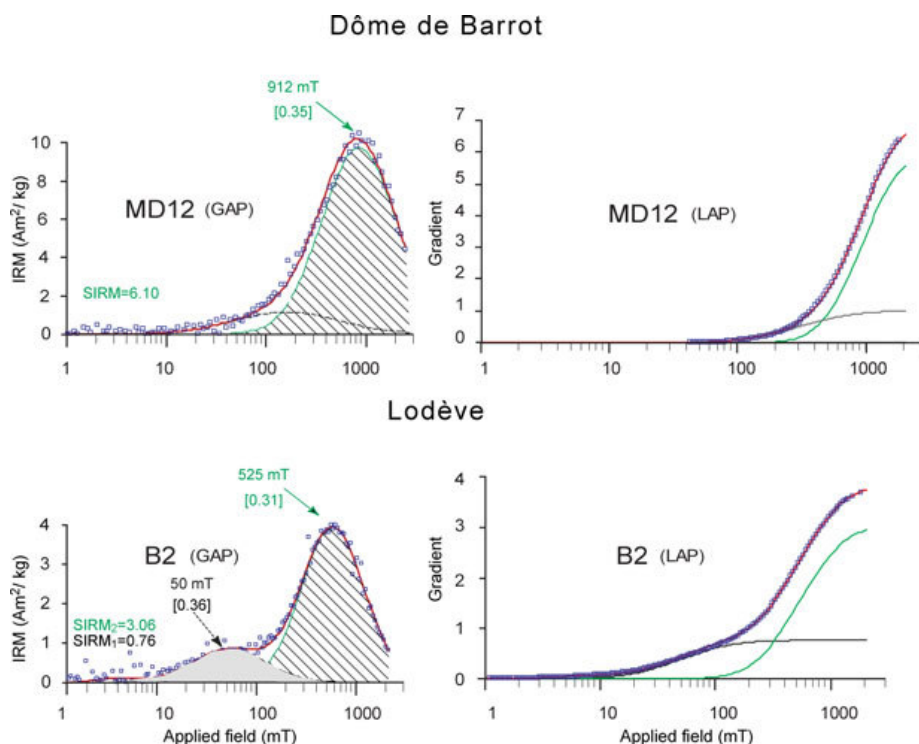


Figure 4. Representative examples of IRM component analysis (Kruiver *et al.* 2001) for samples from Dôme de Barrot and Lodève basin. Blue squares are measured data points. Left-hand panels show examples of an IRM linear acquisition plot (LAP), right-hand panels show the gradient of acquisition plot (GAP). The abscissa (applied field) is logarithmic for both plots. The low coercive contribution in Dôme de Barrot (dashed line in GAP, not labelled) has no physical meaning, but represents the skewness of the distribution (Heslop *et al.* 2004; Egli 2004). The two IRM components from the Lodève are marked with different lines: component 1 (grey line and shading) has a low coercivity and component 2 (green line and hatching) has a high coercivity. Values of the peak field at which half of the SIRM is reached, $B_{1/2}$, are displayed in each panel together with their dispersion parameter (DP) representing one standard deviation.

components are given. In the Dôme de Barrot samples, there is only one main component with a high coercivity, indicative of (specular) haematite. The small component with a low coercivity has no physical meaning; it arises from a skewed data distribution (Heslop *et al.* 2004). In the Lodève samples, two magnetic components are invariably present: a relatively weak low-coercivity component (magnetite/maghemite) and a relatively strong high-coercivity component (haematite).

4.2 NRM demagnetization behaviour

The NRM has been measured on 88 samples from Lodève and 116 samples from Dôme de Barrot; typical examples of demagnetization behaviour in these samples are shown in Fig. 5. The results of the THs were plotted in Zijdeveld diagrams (Zijdeveld 1967), and principal component analysis (Kirschvink 1980) was performed to interpret the directions of NRM. Only components with a maximum angular deviation (MAD) less than 10° were accepted. Apart from the characteristics in the demagnetization diagrams, an indication of the magnetic mineral components can also be deduced from the normalized thermal decay curves of the NRM.

4.2.1 Dôme de Barrot series

The NRM is very stable and the intensities decrease substantially only in the last 15–20 °C before complete unblocking. The maximum unblocking temperature of approximately 680 °C and the

block-shaped decay curves indicate that detrital (specular) haematite is the sole remnance carrier. As shown above in the magnetic mineralogy section, this is consistent with our interpretation of the rock magnetic measurements.

4.2.2 Lodève series

A normal polarity (present day field) component has been recorded in nearly all samples that were entirely removed after heating to 350–400 °C (Fig. 5). At higher temperatures, the behaviour is quite variable: in some samples demagnetization above 480 °C produced spurious behaviour, whereas others survived until 560–580 °C or even higher, up to 650 °C (Fig. 5). Regardless of the variable behaviour at high temperatures, it becomes clear from samples surviving the higher temperatures that the final direction is reliably retrieved after demagnetization to 480–520 °C. The rock magnetic data and the demagnetization behaviour lead us to assume that these red sediments actually bear two high-temperature magnetization components carried by two different magnetic minerals. One is well defined in all samples by an unblocking temperature interval ranging from 460 to 560 °C and suggests that it is carried by maghemite/magnetite being consistent with the low IRM coercivity magnetic mineral seen in the IRM acquisition diagrams (Fig. 4). The other component is not well defined but presumably has higher unblocking temperatures, suggesting that it is carried by haematite, consistent with the red colour of the beds and the high coercivity carriers observed in IRM acquisition diagrams (Fig. 4). In any case, we see that the

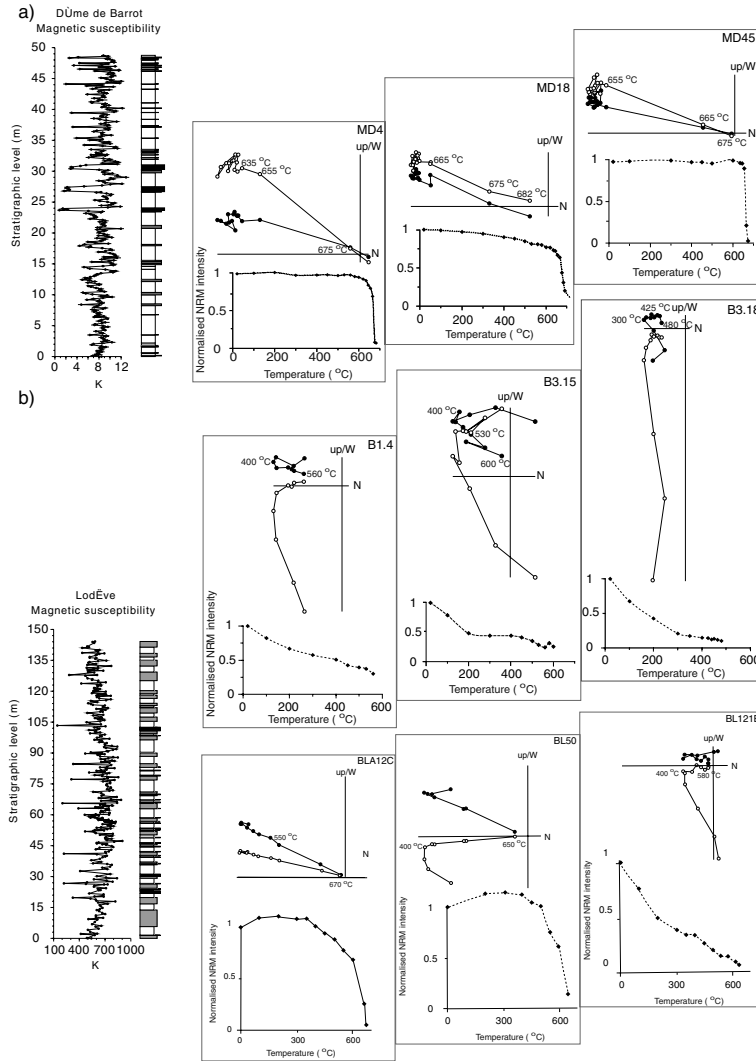


Figure 5. Magnetic susceptibility record of field measurements and the corresponding lithological column, as well as the vector end-point orthogonal diagrams of typical demagnetization behaviour during thermal treatment, for samples from the Dôme de Barrot and Lodève basins. Dark grey bands represent purple lithology (Dôme de Barrot) and indurated, silty lithology (Lodève); white represents red lithology. In the Zijderveld demagnetization diagrams, open (closed) symbols denote projections on the vertical (horizontal) plane. Temperatures are indicated in degrees Celsius for key demagnetization steps. Decay curves for Dôme de Barrot show the typical ‘block-like’ behaviour for specularite, whereas Lodève decay curves show a more gradual decay and two components (discussed in the text).

mineral carrying the ChRM is mostly magnetite/maghemite. When there is also a higher temperature (haematite) component, it has a direction indistinguishable from the magnetite component (e.g. sample BLA12C in Fig. 5).

We supplement our data with results from previously published compilations for Lodève (Kruseman 1962; Merabet & Guillaume 1988; Cogné *et al.* 1990) and Dôme de Barrot (Van den Ende 1977; Kruiver *et al.* 2000). All samples used in the statistics (Table 2) were treated using TH, except the earlier study of Kruseman (1962), in which the samples were AF demagnetized. In nearly all cases, this treatment was sufficient to detect the ChRM component, as we discussed above, since the final direction was already isolated after 480–520 °C.

We provide the directional data from Kruseman (1962), Merabet & Guillaume (1988) and from the thesis of Maillol (1992)

in Table S1, since they are not readily available. The data from Kruseman and Maillol were taken from the original publications, those of Merabet and Guillaume were digitized from their publications. In addition, we separate the data from Maillol (1992) into an older and younger part, according to the formations sampled, and fit them to our new age assignments (Table 1). We plot all data sets from Table 2—including the parametrically sampled data from Cogné *et al.* (1990)—in Fig. S1. The data (from their sites p4, p5 and p6) reported by Cogné *et al.* (1990) have been repositioned in age, based on the location of their sites in the Lodève basin—the previously reported Autunian age must be too old; according to Schneider *et al.* (2006), it should be Kungurian–Wordian (Table 1).

Fig. 6 shows the ChRM directions from our study in equal area projections; the statistical parameters, the number of samples used before and after applying the E/I method and the subsequent

Table 2. Summary of palaeomagnetic results from this study and from literature data for the Dôme de Barrot and Lodève basins. Numbers in the first column are used in Figs 7 and 8.

No.	Study	Method	<i>N</i>	Dec	Inc	<i>K</i>	α_{95}	<i>E</i>	<i>f</i>	<i>S</i> _l	<i>S</i>	<i>S</i> _u
Dôme de Barrot (44.03°N, 6.58°E)												
1	This study and Kruiver <i>et al.</i> (2000) , Roadian	None	206	207.4	−16.3	24.4	2.0	2.74		11.4	12.6	13.8
		TK03	206	207.4	−16.6	24.1	2.0	2.53	0.99	11.5	12.7	13.9
		TK03_vD	199	207.8	−16.8	29.0	1.9	2.70		10.6	11.5	12.2
2	Van den Ende (1972) , Roadian	None	220	206.2	−15.5	34.6	1.6	1.79		9.6	10.6	11.5
		TK03	220	206.2	−18.9	27.9	1.8	2.49	0.79	10.4	11.4	12.3
		TK03_vD	214	206.8	−19.1	29.9	1.8	3.49		9.8	10.5	11.3
3	This study, Kruiver <i>et al.</i> (2000) & Van den Ende (1972) , Roadian	None	426	206.8	−15.9	28.8	1.3	2.22		10.8	11.6	12.4
		TK03	426	206.8	−17.5	26.2	1.4	2.52	0.90	11.2	12.0	12.8
		TK03_vD	411	207.3	−17.5	30.6	1.3	2.53		10.2	10.8	11.3
Lodève (43.69°N, 3.35°E)												
4	This study and Maillol (1992) , Kungurian – Wordian	None	146	199.6	2.1	19.6	2.7	1.62		12.3	14.2	16.1
		TK03	146	199.6	2.7	15.0	3.1	2.81	0.77	13.5	15.4	17.3
		TK03_vD	136	199.8	0.5	20.2	2.8	2.24		11.3	12.5	13.6
5	Maillol (1992) , Sakmarian–Artinskian	None	143	199.6	−7.4	40.6	1.9	1.92		8.2	9.2	10.2
		TK03	143	199.6	−8.9	31.8	2.1	2.70	0.82	9.0	10.0	11.0
		TK03_vD	141	199.6	−8.7	33.3	2.1	2.97		8.7	9.6	10.5
6	Kruseman (1962) , Artinskian – Wordian	None	30	198.9	−4.8	30.2	4.9			8.9	11.3	13.9
		vD	30	198.9	−4.8	30.2	4.9			8.9	11.3	13.9
7	Kruseman (1962) , Sakmarian	None	15	189.9	7.4	47.2	5.6			7.4	9.5	11.7
		vD	15	189.9	7.4	47.2	5.6			7.4	9.5	11.7
8	Merabet & Guillaume (1988) , Artinskian – Wordian	None	93	199.2	−11.1	229.1	1.0			3.7	4.6	5.6
		vD	92	199.4	−11.0	264.5	0.9			3.6	4.1	4.8
9	Merabet & Guillaume (1988) , Sakmarian	None	65	190.7	8.4	112.2	1.7			5.5	6.7	7.9
		vD	63	190.7	8.4	130.2	1.6			5.1	6.0	6.9
10	Cogné <i>et al.</i> (1990) , Kungurian – Wordian	None	22 (p)	194.7	−10.3	33.0	5.6			8.6	10.8	13.0
		vD	22 (p)	194.7	−10.3	33.0	5.6			8.6	10.8	13.0

Notes: *N*, number of samples used in the statistics; dec, declination; inc, inclination; *k*, estimated Fischer precision parameter; α_{95} , half-angle of the cone of confidence at the 95 per cent level; *E*, elongation of the distribution; *f*, the unflattening factor required to meet the *E/I* model TK03.GAD; *S*_l, VGP scatter with lower (*S*_l) and upper (*S*_u) 95 per cent bootstrap (5000×) error limits.

Method is none, no cut-off and no unflattening; TK03; no cut-off and unflattened (TK03 inclination error correction); TK03_vD, TK03 correction and subsequent Vandamme (1994) cut-off; vD, only Vandamme cut-off; (p), parametric sampling.

The TK03 correction has only been applied on data sets with *N* > 100, whereas *E* and *f* are only given for TK03 corrected sets.

Vandamme cut-off are summarized in Table 2. The new Dôme de Barrot data are combined with those of Kruiver *et al.* (2000) (Fig. 7, Table 2); they are from the same outcrop. The combined data set is statistically identical to the data set of Van den Ende (1977) (Fig. 6, Table 2), even though this data set contains an averaged direction per approximate stratigraphic level (five samples per level), which introduces some smoothing. However, since both sets share a common true mean direction ($\gamma = 1.4^\circ < \gamma_c = 2.6^\circ$; classification A), they were combined into a single set. The Lodève data set from this study was combined with the younger data set from Maillol (1992), since they also share a common true mean direction: $\gamma = 4.2^\circ < \gamma_c = 5.5^\circ$, hence classification B. The combined set has *N* = 136 (Table 2) and can be used for the *E/I* method (Fig. 6), whereas the older data set of Maillol (1992) with *N* = 143 was analysed separately. The data sets of the Kruseman (1962) study are divided into two sets of Saxonian and Autunian age (now denoted as Artinskian–Wordian and Sakmarian, respectively; Table 1) since they gave different directions. The small number of samples in these data sets, however, implies that we should be cautious in using them for PSV analysis.

5 DISCUSSION AND CONCLUSIONS

Only the large data sets from Lodève (*N*₁ = 146 and *N*₂ = 143 samples) and Dôme de Barrot (*N* = 426 samples) allow us to test the

directional (and VGP) distributions (Table 2 and Fig. 6). It appears that the observed inclinations do not differ significantly from the inclinations corrected by the model. This can be expected because the sediments were deposited close to the equator, which reduces the effect of flattening. As mentioned above, we have reassessed the ages of earlier studies for the Lodève basin using the new detailed chronology of Schneider *et al.* (2006) (Table 1), taking into account the positions of the sampled sites as reported in those studies. We omit the old terms (Saxonian, Autunian and Thuringian) and replace them with the currently accepted terms and use ages of the new timescale of Menning *et al.* (2006). In Fig. 7, we plot all the results as palaeolatitude against age and compare them with the expected palaeolatitude derived from the apparent polar wander path (APWP) for Europe (Torsvik *et al.* 2008). All results fall within the palaeolatitude/age error window of this APWP. We also plot the corrected palaeolatitudes and their errors according to the inclination error correction of TK03.GAD for the data sets with *N* > 100. This does not give a significant difference, as mentioned above. The results of Cogné *et al.* (1990) now fit the palaeolatitude derived from the APWP very well, whereas it previously did not because of an erroneous age assignment.

In Table 2, we also give the elongations *E* of the original, unflattened and cut-off distributions and the flattening factor *f* required to obtain the elongation required by the TK03.GAD model. The Dôme de Barrot data of this study requires no unflattening (*f* = 0.99) to

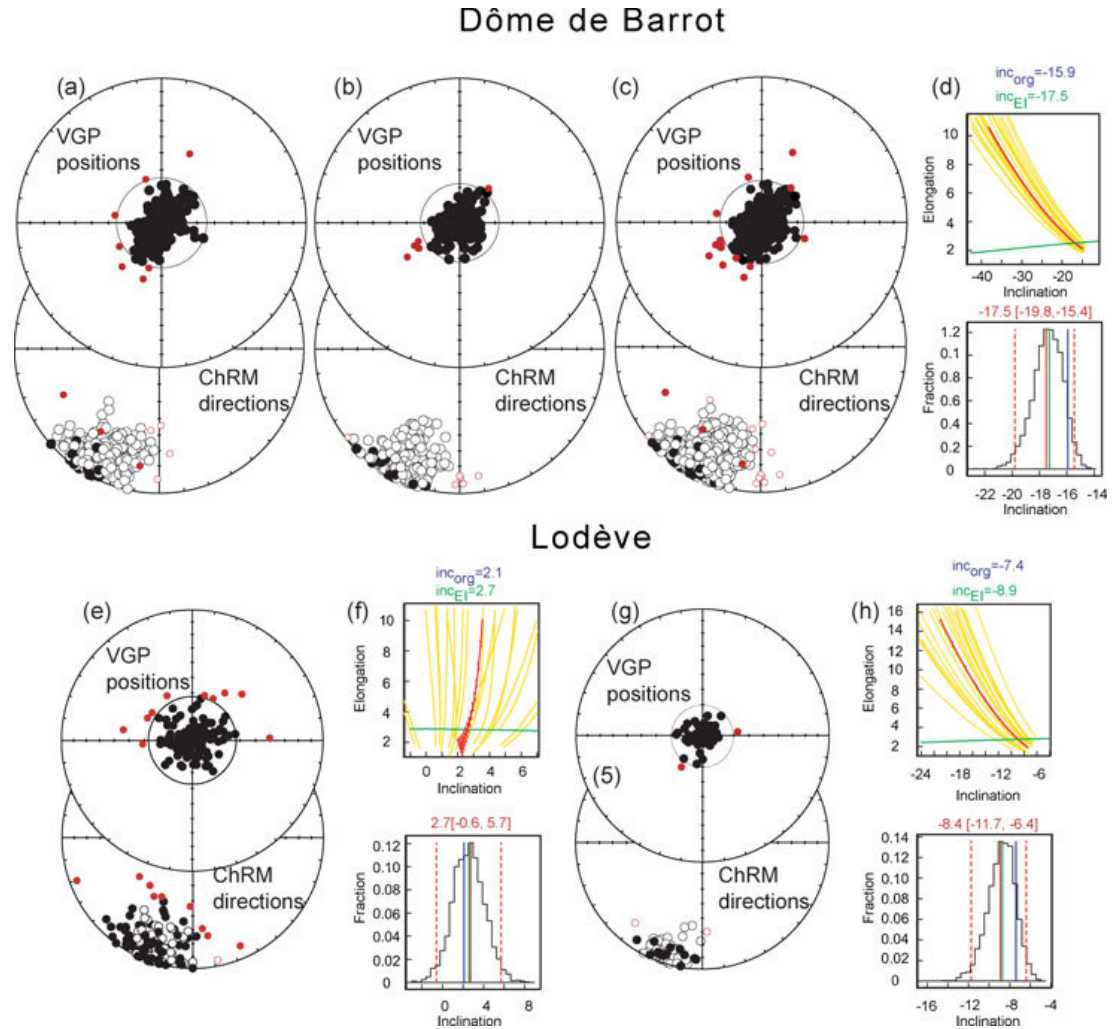


Figure 6. Equal area plots of the unflattened directions—using TK03.GAD—together with the corresponding VGPs shown with respect to their mean for samples from Dôme de Barrot and from Lodève basin. Small symbols are the data cut-off by using the Vandamme (1994) method. Open/closed symbols indicate negative/positive inclinations; the statistics of the data are listed in Table 2. Also shown are the plots of elongation versus inclination of the distribution upon increasing unflattening (red solid line) by using the TK03.GAD model (Tauxe & Kent 2004); bars give the direction of the long axis of elongation with horizontal being E–W and vertical being N–S; green line represents the model E/I ratio. Where the line intersects the model, one finds the inclination–elongation pair most consistent with the TK03.GAD model and the corresponding unflattened inclination inc_{EI} ; the original inclination inc_{org} is also given. Also shown are results (yellow lines) from 20 (out of 5000) bootstrapped data sets. Below the E/I panels, histograms of crossing points from 5000 bootstrapped data sets are shown. The most frequent inclination (solid red vertical line; dashed red vertical lines denote the 95 per cent bootstrap error) is given as value (and 95 per cent significance range) on top of the panel; the inclinations of the original distribution (blue vertical line) and the intersection with the model (green vertical line) are indicated. In no case, the inclination correction is significant, but always within the 95 per cent error limits.

arrive at the required elongation, whereas the other data sets require some unflattening. In no case, however, is a significant correction of the inclination obtained, and unflattened inclinations fall within 95 per cent bootstrap errors.

In Fig. 8(a), the VGP scatter from Lodève and Dôme de Barrot red beds is compared with the VGP scatter derived from low-latitude lavas for the last 5 Myr included in the PSVRL database (McElhinny & McFadden 1997). The S values we measured from the Permian red beds of Lodève and Dôme de Barrot are consistent with one another and with the results of several other published studies. Furthermore, these values agree (within error) with the scatter predicted by two published models of PSV: Model G (McFadden *et al.* 1988) and TK03.GAD (Tauxe & Kent 2004). The

S values of the Merabet & Guillaume (1988) study are significantly lower for the corresponding palaeolatitude. However, since all other data sets from the same sediments yield much higher S values, we do not consider these as reliable measurements of the VGP scatter caused by secular variation. Rather, we suspect that these values of S were artificially suppressed by, most likely, an insufficient temporal sampling of the secular variation.

The PSVRL database has been superseded by the time-averaged field initiative (TAFI). A very recent study (Johnson *et al.* 2008) collated TAFI and other recently published data and, using strict criteria, found that their VGP scatter was higher at low latitudes than reported by McElhinny & McFadden (1997) and less dependent on latitude. They concluded this after subjecting their data to a

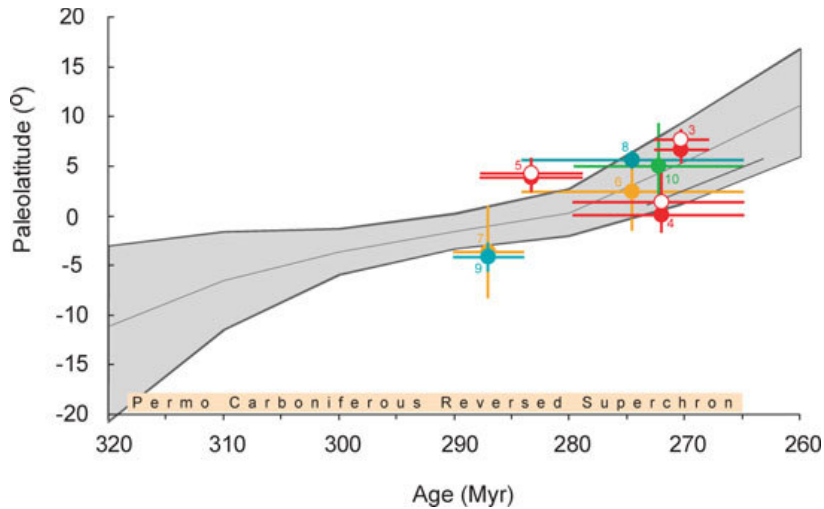


Figure 7. Ages and their errors corrected according to Table 1 versus palaeolatitude showing the Torsvik *et al.* (2008) apparent polar wander path (grey line plus shaded error margins). All directions and the corresponding palaeolatitudes are pole corrected with respect to the Lodève basin (43.69°N, 3.35°E). Open symbols represent TKO3.GAD corrected palaeolatitudes. The numbers refer to those in Table 2.

fixed (45°) cut-off. They also tested the Vandamme variable cut-off and found no significant differences. In Fig. 8(b), we plot our data (treated with a fixed 45° cut-off instead of variable cut-off, to be comparable with the Johnson *et al.* 2008 study) and compare them with this compilation. Model G is a phenomenological model of PSV, which uses two ‘shape parameters’ to define a quadratic curve, which is then fit (by the least-squares technique) to a set of VGP scatter data plotted against (palaeo)latitude. We used this approach in combination with the bootstrap method of uncertainty estimation to determine the best fit plus the 95 per cent bootstrap errors through Johnson *et al.*’s (2008). data. Here, each of the 1000 bootstraps takes a random sample within the published error limits of each individual data point and fits a line to it.

It is evident that now our data fall significantly below those from the last 5 Myr at low latitudes (less than 25°–30°), suggesting that PSV was effectively reduced at low latitudes during the PCRS. The scatter observed at low latitudes in this study is considerably higher than that found by McFadden *et al.* (1991) in their study of the CNS. This could be because the process causing the PCRS is different from the one causing the CNS (Larson 1991; Courtillot & Valet, 1995; Greff-Lefftz & Legros 1999). However, a very recent and updated study of PSV in the CNS (Biggin *et al.* 2008b) concluded that McFadden *et al.*’s (1991) measurements of low-latitude VGP scatter in the CNS were probably biased, and that the actual scatter was higher (although still significantly lower than that observed for the past 5 Myr). In Fig. 8(b), we plot the Model G curve, which is fit to the highest quality ‘Group 1’ data set of this recently updated study of the CNS. There is evidently a much better correlation with the VGP scatter observed at low latitudes during the CNS than for the VGP scatter of the last 5 Myr. This strongly suggests that there is indeed a reduced VGP scatter during a superchron at low latitudes, in turn suggesting that the contribution of the even spherical harmonics is notably reduced. Every palaeomagnetic data set has some error associated with it, which is derived from the sampling and measuring process, and this will contribute to the measured VGP scatter. In PSV studies performed on lavas, some estimate of this additional scatter can be calculated from the within-site scatter, measured between samples from the same (rapidly cooled) lava flows. In PSV

records from sedimentary rocks, this is not possible because each sample reflects an unknown interval of time. Biggin *et al.* (2008b) numerically simulated the effects of combined scatters due to measurement and geomagnetic sources. They found that for modest degrees of random Fisher-distributed errors introduced in direction space ($\kappa = 182$), the effect of not applying any within-site error correction would be to introduce a strongly latitudinal-dependent artefact to the observed VGP scatter (see their figs 3c and d). Fortunately, this effect is relatively small (1°–2° of enhanced scatter) at sites from low palaeolatitudes and therefore is unlikely to influence the findings of this study. Furthermore, one of the main results of the present study is that the VGP scatter was observed to be lower (at low latitudes) during the PCRS than it was in the last 5 Myr. This conclusion would only be strengthened by consideration of possible unremoved biasing effects from random errors.

We have examined the PSV during the PCRS at low equatorial latitudes by evaluating the VGP scatter recorded by the red beds from two Permian basins. The results of this study agree remarkably well with several others from the same basins, even though some of the published data sets are small (Kruseman 1962; Cogné *et al.* 1990). This suggests that the observed VGP scatter is a robust feature that is well recorded. Our measurements of VGP scatter agree well with those produced from the PSVRL database for the last 5 Myr and with the predictions of a recent model of the field (TKO3.GAD). However, they are significantly lower than those measured by a recent study using an updated database of lavas from the last 5 Myr (Johnson *et al.* 2008).

Our findings, similar to those of Biggin *et al.* (2008b), show that secular variation at low latitudes, as expressed by VGP scatter, was likely lower in a superchron than in a period of higher reversal frequency. In a subsequent paper, we report all available sedimentary records from the PCRS, using the approach outlined here.

ACKNOWLEDGMENTS

We thank Tom A. T. Mullender for technical assistance and Dave Heslop for carrying out the new spectral analysis of the Dôme de Barrot susceptibility record and for providing Fig. 2. The reviews of

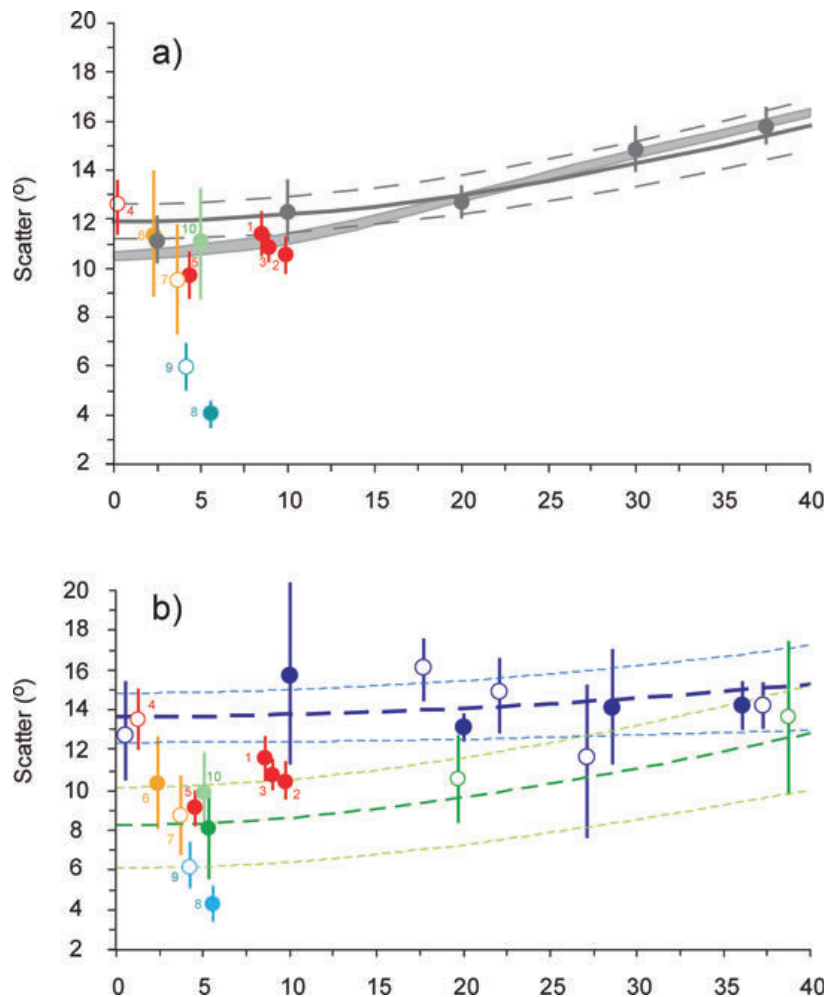


Figure 8. (a) VGP scatter after using the Vandamme cut-off of the Permian data sets versus latitude, compared with the palaeosecular variation database of 0–5 Myr lavas (dark grey dots). Model G of McElhinny & McFadden (1997) is a dark grey line, with dashed grey lines denoting 95 per cent error bounds. The PSV scatter according to TKO3.GAD is a light grey shaded line. (b) VGP scatter (using 45° fixed cut-off) of the Permian data sets versus latitude, compared with the results of 0–5 Myr lavas (Johnson *et al.* 2008); blue symbols; closed (open) symbols refer to data from the Northern (Southern) Hemisphere. Blue dashed line denotes a Model G approach through their data; small dashed lines denote 95 per cent bootstrap error bounds. Also shown is the data from the recent compilation for the CNS (Biggin *et al.* 2008a, b); green symbols represent their Group 1 data; open and closed symbols, large and small dashed lines, as above for the recent lavas. Numbers refer to those in Table 2.

Rob van der Voo and Lisa Tauxe considerably improved an earlier manuscript. This work was funded by the Netherlands Organisation for Scientific Research (NWO) and was conducted under the program of the Vening Meinesz research School of Geodynamics (VMSG).

REFERENCES

- Berger, A., Loutre, M.F. & Laskar, J., 1992. Stability of the astronomical frequencies over the Earth's history for paleoclimate studies, *Science*, **255**, 560–566.
- Biggin, A.J., Strik, G.H.M.A. & Langereis, C.G., 2008a. Evidence for a very-long-term trend in geomagnetic secular variation, *Nat. Geosci.*, **1**(6), 395–398.
- Biggin, A.J., Van Hinsbergen, D.J.J., Langereis, C.G., Straathof, G.B. & Deenen, M.H.L., 2008b. Geomagnetic secular variation in the Cretaceous Normal Superchron and in the Jurassic, *Phys. Earth planet. Inter.*, **169**(1–4), 3–19.
- Blow, R.A. & Hamilton, N., 1978. Effect of compaction on the acquisition of a detrital remanent magnetization in fine-grained sediments, *Geophys. J. R. astr. Soc.*, **52**, 13–23.
- Bordet, P., 1950. Le Dôme permien de Barrot (Alpes-Maritimes) et son auréole de terrains secondaires, *Bull. Serv. Carte Géol. France*, **228**(XLVIII), 51–90.
- Brown, M.C., Holme, R. & Bargery, A., 2007. Exploring the influence of the non-dipole field on magnetic records for field reversals and excursions, *Geophys. J. Int.*, **168**(2), 541–550.
- Coe, R.S. & Glatzmaier, G.A., 2006. Symmetry and stability of the geomagnetic field, *Geophys. Res. Lett.*, **33**(21), L21311.
- Coe, R.S., Hongre, L. & Glatzmaier, G.A., 2000. An examination of simulated geomagnetic reversals from a palaeomagnetic perspective, *Phil. Trans. R. Soc. Lond., A (Mathematical Physical and Engineering Sciences)*, **358**(1768), 1141–1170.
- Cogné, J.P., Brun, J.P. & Vandendriessche, J., 1990. Paleomagnetic

- evidence for rotation during Stephano-Permian extension in southern Massif-Central (France), *Earth planet. Sci. Lett.*, **101**(2-4), 272–280.
- Constable, C.G. & Johnson, C.L., 2005. A Paleomagnetic Power Spectrum, *Phys. Earth planet. Inter.*, **153**, 61–73.
- Constable, C.G. & Parker, R.L., 1988. Statistics of the geomagnetic secular variation for the past 5 m.y., *J. geophys. Res.*, **93**(B10), 11 569–11 581.
- Courtilot, V. & Valet, J.-P., 1995. Secular variation of the Earth's magnetic field: from jerks to reversals, *Comptes rendus de l'Académie des Sciences (Paris), Série II*, **320**, 903–922.
- Cox, A., 1970. Latitude dependence of the angular dispersion of the geomagnetic field, *Geophys. J. R. astron. Soc.*, **20**, 253–269.
- de Boer, C.B. & Dekkers, M.J., 1998. Thermomagnetic behaviour of haematite and goethite as a function of grain size in various non-saturating magnetic fields, *Geophys. J. Int.*, **133**, 541–552.
- de Boer, C.B. & Dekkers, M.J., 2001. Unusual thermomagnetic behaviour of haematites: neoformation of a highly magnetic spinel phase on heating in air, *Geophys. J. Int.*, **144**, 481–494.
- Dunlop, D.J. & Özdemir, Ö., 1997. *Rock Magnetism: Fundamentals and Frontiers*, Cambridge University Press, Cambridge.
- Egli, R., 2004. Characterization of individual rock magnetic components by analysis of remanence curves, 2: fundamental properties of coercivity distributions, *Phys. Chem. Earth*, **29**(13–14 Spl. Iss.), 851–867.
- Glatzmaier, G.A. & Olson, P., 2005. Probing the geodynamo, *Sci. Am.*, **292**(4), 50–57.
- Glatzmaier, G.A. & Roberts, P.H., 1995. A three-dimensional convective dynamo solution with rotating and finitely conducting inner core and mantle, *Phys. Earth planet. Inter.*, **91**, 63–75.
- Glatzmaier, G.A., Coe, R.S., Hongre, L. & Roberts, P.H., 1999. The role of the Earth's mantle in controlling the frequency of geomagnetic reversals, *Nature*, **401**(6756), 885–890.
- Glenister, B.F., Wardlaw, B.R. & Lambert, L.L. *et al.*, 1999. Proposal of Guadalupian and component Roadian, Wordian and Capitanian stages as international standards for the Middle Permian Series, *Permophiles*, **34**, 3–11.
- Gradstein, F., Ogg, J. & Smith, A. (eds), 2004. *A Geologic Time Scale*, Cambridge University Press, Cambridge, UK.
- Greff-Lefftz, M. & Legros, H., 1999. Core rotational dynamics and geological events, *Science*, **286**, 1707–1709.
- Grommé, S., Wright, T.L. & Peck, D.L., 1969. Magnetic properties and oxidation of iron-titanium oxide minerals in Alae and Makaopuhi lava lakes, Hawaii, *J. geophys. Res.*, **74**, 5277–5294.
- Heslop, D., McIntosh, G. & Dekkers, M.J., 2004. Using time- and temperature-dependent Preisach models to investigate the limitations of modelling isothermal remanent magnetization acquisition curves with cumulative log Gaussian functions, *Geophys. J. Int.*, **157**(1), 55–63.
- Hollerbach, R. & Jones, C.A., 1993. Influence of the Earth's inner core on geomagnetic fluctuations and reversals, *Nature*, **365**, 541–543.
- Johnson, C.L. *et al.*, 2008. Recent investigations of the 0–5 Ma geomagnetic field recorded by lava flows, *Geochem. Geophys. Geosyst.*, **9**(Q04032), doi:10.1029/2007GC001696.
- Kent, D.V. & Smethurst, M.A., 1998. Shallow bias of paleomagnetic inclinations in the Paleozoic and Precambrian, *Earth planet. Sci. Lett.*, **160**, 391–402.
- Kent, D.V. & Tauxe, L., 2005. Corrected Late Triassic latitudes for continents adjacent to the North Atlantic, *Science*, **307**(5707), 240–244.
- King, R.F., 1955. Remanent magnetism of artificially deposited sediments, *Mon. Not. R. Astron. Soc. Geophys. Suppl.*, **7**, 115–134.
- King, T., 1996. Quantifying nonlinearity and geometry in time series of climate, *Quat. Sci. Rev.*, **15**, 247–266.
- King, R.F. & Rees, A.I., 1966. Detrital magnetism in sediments: an examination of some theoretical models, *J. geophys. Res.*, **71**, 561–571.
- Kirschvink, J.L., 1980. The least-squares line and plane and the analysis of paleomagnetic data, *Geophys. J. R. astron. Soc.*, **62**, 699–718.
- Krijgsman, W. & Tauxe, L., 2004. Shallow bias in Mediterranean paleomagnetic directions caused by inclination error, *Earth planet. Sci. Lett.*, **222**(2), 685–695.
- Kruiver, P.P., Dekkers, M.J. & Langereis, C.G., 2000. Secular variation in Permian red beds from Dome de Barrot, SE France, *Earth planet. Sci. Lett.*, **179**(1), 205–217.
- Kruiver, P.P., Dekkers, M.J. & Heslop, D., 2001. Quantification of magnetic coercivity components by the analysis of acquisition curves of isothermal remanent magnetisation, *Earth planet. Sci. Lett.*, **189**(3-4), 269–276.
- Kruiver, P.P., Langereis, C.G., Dekkers, M.J., Davies, G.R. & Smeets, R.J., 2002. The implications of non-suppressed geomagnetic secular variation during the Permo-Carboniferous Reversed Superchron, *Phys. Earth planet. Inter.*, **131**(3-4), 225–235.
- Kruseman, G.P., 1962. Étude paléomagnétique et sédimentologique du bassin Permian de Lodève-Hérault, France, *Geologica Ultraiectina*, **9**, 1–65.
- Larson, R.L., 1991. Geological consequences of superplumes, *Geology*, **19**, 963–966.
- Laskar, J., 1990. The chaotic motion of the solar system: a numerical estimate of the size of the chaotic zones, *Icarus*, **88**, 266–291.
- Maillol, J.M., 1992. A paleomagnetic investigation of the Permo-Carboniferous Superchron, *PhD thesis*. University of Alberta.
- Maillol, J.M. & Evans, M.E., 1993. Permian palaeosecular variation as recorded in the Lodève redbeds, southern France, *Geologica Carpathica*, **44**(5), 281–287.
- McElhinny, M.W. & McFadden, P.L., 1997. Palaeosecular variation over the past 5 Myr based on a new generalized database, *Geophys. J. Int.*, **131**(2), 240–252.
- McElhinny, M.W. & Merrill, R.T., 1975. Geomagnetic secular variation over the past 5 million years, *Rev. Geophys. Space. Phys.*, **13**, 687–708.
- McFadden, P.L. & McElhinny, M.W., 1988. The combined analysis of remagnetization circles and direct observations in paleomagnetism, *Earth planet. Sci. Lett.*, **87**, 161–172.
- McFadden, P.L. & McElhinny, M.W., 1990. Classification of the reversal test in paleomagnetism, *Geophys. J. Int.*, **103**, 725–729.
- McFadden, P.L. & Merrill, R.T., 1995. History of Earth's magnetic field and possible connections to core-mantle boundary processes, *J. geophys. Res.*, **100**, 307–316.
- McFadden, P.L., Merrill, R.T. & McElhinny, M.W., 1988. Dipole quadrupole family modeling of Paleosecular variation, *J. geophys. Res.*, **93**(B10), 11 583–11 588.
- McFadden, P.L., Merrill, R.T., McElhinny, M.W. & Lee, S., 1991. Reversals of the Earth's magnetic field and temporal variations of the dynamo families, *J. geophys. Res. B—Solid Earth*, **96**, 3923–3933.
- Menning, M. *et al.*, 2006. Global time scale and regional stratigraphic reference scales of Central and West Europe, East Europe, Tethys, South China, and North America as used in the Devonian-Carboniferous-Permian Correlation Chart 2003 (DCP 2003), *Palaeogeogr. Palaeoclimatol. Palaeoecol.*, **240**(1-2), 318–372.
- Menning, M. *et al.*, 2001. The optimal number of Carboniferous series and stages, *Newslet. Stratigr.*, **38**(2-3), 201–207.
- Merabet, N. & Guillaume, A., 1988. Paleomagnetism of the Permian Rocks of Lodève (Hérault, France), *Tectonophysics*, **145**(1-2), 21–29.
- Mullender, T.A.T., van Velzen, A. J. & Dekkers, M. J., 1993. Continuous drift correction and separate identification of ferrimagnetic and paramagnetic contributions in thermomagnetic runs, *Geophys. J. Int.*, **114**, 663–672.
- Ogg, J.G., Agterberg, F.P. & Gradstein, F.M., 2004. The Cretaceous Period, in *A Geologic Time Scale 2004*, eds Gradstein, F.M., Ogg, J.G. & Smith, A.G., Cambridge University Press, Cambridge, p. 589.
- Opdyke, N.D., Roberts, J., Claoué-Long, J., Irving, E. & Jones, P. J., 2000. Base of the Kiaman: its definition and global stratigraphic significance, *GSA Bull.*, **112**(9), 1315–1341.
- Paillard, D., Labeyrie, L. & Yiou, P., 1996. Analyseries 1.1—Macintosh program performs time-series analysis, *EOS*, **77**, 379.
- Quidelleur, X. & Courtilot, V., 1996. On low-degree spherical harmonic models of paleosecular variation, *Phys. Earth planet. Inter.*, **95**(1-2), 55–77.
- Roberts, A.P., Cui, Y. & Verosub, K.L., 1995. Wasp-waisted hysteresis loops: mineral magnetic characteristics and discrimination of components in mixed magnetic systems, *J. geophys. Res.*, **100**(B9), 17 909–17 924.

- Schneider, J.W., Korner, F., Roscher, M. & Kroner, U., 2006. Permian climate development in the northern peri-Tethys area—the Lodeve basin, French Massif Central, compared in a European and global context, *Palaeogeogr. Palaeoclimatol. Palaeoecol.*, **240**(1-2), 161–183.
- Spassov, S., Heller, F., Kretzschmar, R., Evans, M.E., Yue, L.P. & Nourgaliev, D.K., 2003. Detrital and pedogenic magnetic mineral phases in the loess/palaesol sequence at Lingtai (Central Chinese Loess Plateau), *Phys. Earth planet. Inter.*, **140**(4), 255–275.
- Steiner, M.B., 1983. Detrital remanent magnetization in hematite, *J. geophys. Res. B—Solid Earth*, **88**, 6523–6539.
- Tauxe, L. & Badgley, C., 1984. Transition stratigraphy and the problem of remanence lock-in times in the Siwalik Red Beds, *Geophys. Res. Lett.*, **11**, 611–613.
- Tauxe, L. & Kent, D.V., 1984. Properties of a detrital remanence carried by hematite from a study of modern river deposits and laboratory redeposition experiments, *Geophys. J. R. astr. Soc.*, **77**, 543–561.
- Tauxe, L. & Kent, D.V., 2004. A simplified statistical model for the geomagnetic field and the detection of shallow bias in paleomagnetic inclinations: was the ancient magnetic field dipolar?, *Geophys. Monogr.*, **145**, 101–116.
- Tauxe, L., Mullender, T.A.T. & Pick, T., 1996. Potbellies, wasp-waists, and superparamagnetism in magnetic hysteresis, *J. geophys. Res.*, **101**(B1), 571–583.
- Tauxe, L., Kodama, K.P. & Kent, D.V., 2008. Testing corrections for paleomagnetic inclination error in sedimentary rocks: a comparative approach, *Phys. Earth planet. Inter.*, **169**(1-4), 152–165.
- Torsvik, T.H., Dietmar Müller, R., Van Der Voo, R., Steinberger, B. & Gaina, C., 2008. Global plate motion frames: toward a unified model, *Rev. Geophys.*, **46**, RG3004, doi:10.1029/2007RG000227.
- Valet, J.-P., Plenier, G., 2008. Simulations of a time-varying non-dipole field during geomagnetic reversals and excursions, *Phys. Earth planet. Inter.*, **169**(1-4), 178–193.
- Vandamme, D., 1994. A new method to determine paleosecular variation, *Phys. Earth planet. Inter.*, **85**, 131–142.
- Van Den Ende, C., 1970. Secular variation in Permian Redbeds from the Dome de Barrot (France), in *Palaeogeophysics*, pp. 101–116, ed. Runcorn, S.K., Academic Press, London.
- Van Den Ende, C.V., 1977. Palaeomagnetism of Permian Red Beds of the Dôme de Barrot – (S. France), *PhD thesis*. Utrecht University, 171 pp.
- Van Der Voo, R. & Torsvik, T.H., 2001. Evidence for the late Paleozoic and Mesozoic non-dipole fields provides an explanation for the Pangea reconstruction problems, *Earth planet. Sci. Lett.*, **187**, 71–81.
- Visscher, H., Huddleston Slater-Offerhaus, M.G. & Wong, T.E., 1974. Palynological assemblages from “Saxonian” deposits of the Saar-Nahe Basin (Germany) and the Dôme de Barrot (France)—an approach to chronostratigraphy, *Rev. Palaeobot. Palynol.*, **17**, 39–56.
- Watson, G.S., 1983. Large sample theory of the Langevin distribution, *J. Stat. Plan. Inference*, **8**, 245–256.
- Zijderveld, J.D.A., 1967. A.C. Demagnetization of rocks: analysis of results, in *Methods in Palaeomagnetism*, pp. 254–286, eds Collinson, D.W., Creer, K.M. & Runcorn, S.K. Elsevier, New York.

SUPPORTING INFORMATION

Additional Supporting Information may be found in the online version of the article.

Figure S1. All data sets from Table 2 are plotted in this figure.

Table S1. Directional data not readily available elsewhere.

Please note: Wiley-Blackwell are not responsible for the content or functionality of any supporting materials supplied by the authors. Any queries (other than missing material) should be directed to the corresponding author for the article.